The modeling of excimer laser particle removal from hydrophilic silicon surfaces

X. Wu, E. Sacher[a], and M. Meunier
Groupe de Recherche en Physique et Technologie des Couches Minces, Département de Génie Physique et de Génie des Matériaux, École Polytechnique de Montréal, C.P. 6079, Succursale Centre-Ville, Montréal, Québec H3C 3A7, Canada

(Received 19 July 1999; accepted for publication 18 January 2000)

We summarize experimental results on the successful removal of submicron-sized polystyrene latex, carboxylate-modified latex, SiO_2, and Al_2O_3 particles from hydrophilic silicon surfaces by excimer laser, using both dry and steam cleaning; the cleaning and damage thresholds have also been determined for these particles. Adhesion and removal models for an ideal sphere particle, that include van der Waals forces, hydrogen bonding, and thermoelastic effects, theoretically explain the laser cleaning results. Two models of the removal force due to the explosive evaporation of liquid film have been calculated and compared. The effects of both asperities on the particle surface and particle aggregation have also been considered. The results of the calculations show that even those surface asperities which are small compared with the particle dimension can cause a large reduction in both adhesion and thermoelastic removal forces. The theoretical predictions are consistent with the experimental observations. © *2000 American Institute of Physics.* [S0021-8979(00)06008-4]

I. INTRODUCTION

The interaction of an excimer laser with a silicon surface can lead to the removal of submicron-sized contaminant particles.[1,2] This technique is efficient, simple, fast, and chlorofluorocarbon-free, which have considerable environmental advantages over standard cleaning techniques. Laser cleaning may be dry, meaning that no energy transfer liquid is present on the sample surface during laser exposure; dry laser cleaning is compatible with cluster tools. However, to increase particle removal efficiencies, steam laser cleaning may be used. During steam cleaning, the laser energy is absorbed by the substrate surface and the surface temperature rises rapidly. The energy from the substrate surface is coupled to a liquid energy transfer medium, such as water, which is condensed on the silicon surface just prior to the arrival of the laser pulse,[3–5] which results in the explosive evaporation of the liquid. We have also used our excimer laser cleaning technique for the removal of metallic contaminates from the backsides of silicon wafers.[6]

The particle removal efficiency of laser cleaning depends on two major factors: the adhesion forces holding the particles to the substrate surface and the laser-induced particle removal forces. It is well established that the laser cleaning efficiency increases with increasing laser fluence[5] but, at very high laser fluences, substrate surfaces are easily damaged by laser irradiation.[5,7,8] Thus, determining the optimal laser cleaning conditions and clearly understanding the interaction mechanisms between particle and substrate surface are the goals of our modeling of the laser cleaning process.

Many studies have been carried out to unravel the interactions that occur in particulate adhesion and removal.[9–15] Most of them considered either adhesion or removal. In our present article, we do both. First, we summarize the experimental results of the removal of submicron-sized particles, such as SiO_2, Al_2O_3, polystyrene latex (PSL), and carboxylate-modified latex (CML), from hydrophilic silicon surfaces by pulsed excimer laser irradiation; the cleaning and damage thresholds of the particles were also determined. Then, in order to obtain a total picture of both particle adhesion and removal by laser cleaning, these results are rationalized through an analysis of adhesion and removal forces. These forces include van der Waals, capillary and chemical forces, as well as rapid thermal expansion and bubble generation pressure forces. Further, by comparing the cleaning results of two kinds of SiO_2 particles having different surface roughnesses, we were able to show that particle surface asperities have a substantial effect on the cleaning efficiency; our theoretical models of adhesion and removal include these effects.

II. SUMMARY OF EXCIMER LASER CLEANING RESULTS AND PHOTOACOUSTIC WAVE MEASUREMENTS

Details of the excimer laser cleaning and photoacoustic wave (PAW) measurement systems have been described elsewhere,[16,17] and the reader is referred to these articles for precise information. Briefly, a KrF excimer laser (MPB Technologies, Inc., AQX-150, operating at 248 nm with a 22 ns pulse full width at half maximum and a fluence of 200 mJ) was used to irradiate the hydrophilic silicon surfaces[8] on which 0.1 μm SiO_2, 0.1 μm Al_2O_3, 0.1 μm PSL, or 0.2 μm CML particles were deposited. A laser scanning surface inspection system (Particle Measuring Systems, Inc., SAS 3600) was used to determine the particle densities on the wafer surfaces, before and after laser cleaning. The PAW signals were detected by a broadband piezoelectric transducer (Panametrics, V1091) which contacted the backside of the silicon wafer. They were amplified by a preamplifier (HP

[a]Electronic mail: sacher@email.phys.polymtl.ca

 © 2000 American Institute of Physics

Downloaded 06 May 2002 to 132.204.56.47. Redistribution subject to AIP license or copyright, see http://ojps.aip.org/japo/japcr.jsp

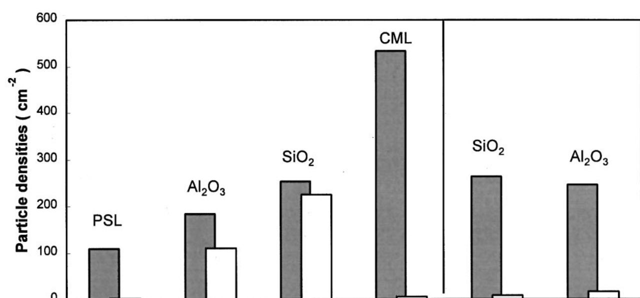

FIG. 1. Particle densities before (gray bar) and after (white bar) laser cleaning. During dry laser cleaning, the laser energy fluxes for PSL, SiO_2, Al_2O_3, and CML were 326, 314, 326, and 353 mJ/cm^2, respectively, and 2, 4, 4, and 2 cleaning scanning cycles were used, respectively. During steam cleaning, the laser energy fluxes for SiO_2 and Al_2O_3 were 180 and 154 mJ/cm^2, respectively, and 5 and 4 cleaning scanning cycles were used, respectively.

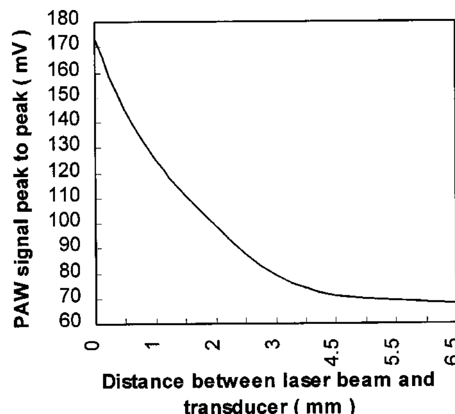

FIG. 3. The peak-to-peak amplitude of the PAW signal as a function of the distance between the laser beam and the transducer located at the backside of the silicon wafer of during dry cleaning with a laser flux of 321 mJ/cm^2.

8447A) and displayed on a 300 MHz digitizing oscilloscope (HP 54201D), before being analyzed by computer.

The removal of particles is localized in the laser beam during both dry and steam cleaning. Figure 1 shows the particle densities, before and after laser irradiation, for both dry and steam cleaning. The results show that the organic particles, PSL and CML, were effectively removed by dry cleaning with a laser flux near 320 mJ/cm^2. However, the inorganic particles, SiO_2 and Al_2O_3, of the same size, were much less efficiently cleaned; they were removed with high efficiencies only on steam cleaning. The particles remaining after laser cleaning may have been due to several sources: strongly adhering particles, recontamination by the ejected particles near the surface, a transfer from adjacent uncleaned areas, and contamination by the cleaning system.

We have shown that the PAW signal induced by the laser pulse propagates along the silicon wafer surface, perpendicular to the long axis of the laser beam, and is reflected at the wafer edge.[16,17] Our study further showed that the amplitude of the PAW signal strongly depends on the incident laser energy, the cleaning method and the distance between the laser beam and the location of the transducer, as indicated in Figs. 2 and 3. It should be noted that the PAW signal cannot be measured where the laser beam strikes, and the values there are clearly much larger than what we measure.

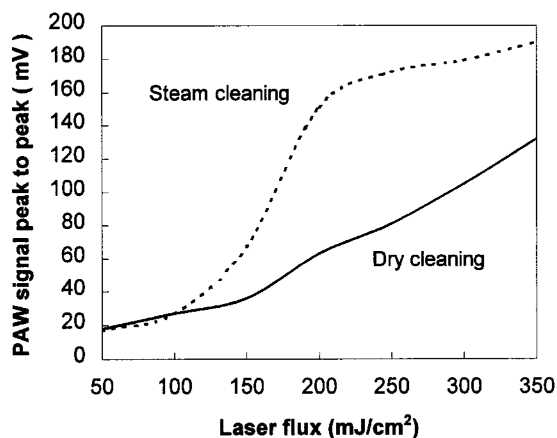

FIG. 2. The peak-to-peak amplitude of the PAW signal as a function of incident laser flux during dry and steam cleaning.

III. LASER CLEANING THRESHOLDS

There is no common definition for the laser cleaning threshold because it strongly depends on the particle diameter and the initial particle density on the substrate surface. In our study, the particle diameter was 0.1 μm and the initial particle density was about 200 cm^{-2}, which is similar with that of a heavily contaminated wafer. The cleaning threshold is defined here as the removal of 50% of the particles from the substrate surface. In Table I, we list the cleaning and damage thresholds, during dry and steam cleaning, for PSL, SiO_2, and Al_2O_3.

The cleaning threshold of PSL during dry cleaning, 76 mJ/cm^2, was much lower than the optimal cleaning condition, 340 mJ/cm^2. To obtain a high cleaning efficiency, more laser energy is needed to remove those particles which are more tenaciously held at the surface, to eject the particles more farther away, and to reduce the number of multiple scans necessary, to minimize recontamination.

It is interesting to note that SiO_2 and Al_2O_3 particles have the same cleaning thresholds during steam cleaning, 143 mJ/cm^2. It was at this flux that we also observed the onset of explosive evaporation of the water film, very close to the optimal cleaning flux of 150 mJ/cm^2. This phenomenon demonstrates that bubble pressure plays an important role in the removal of inorganic oxide particles. To explain the large differences between dry and steam cleaning, and between particle types and cleaning thresholds, we quantitatively analyze the adhesion and removal forces between particles and substrate surfaces.

TABLE I. Cleaning and damage thresholds.

Particles	PSL (0.1 μm)	SiO_2 (0.1 μm)	Al_2O_3 (0.1 μm)
Laser cleaning method	Dry	Steam	Steam
Laser cleaning threshold	76 mJ/cm^2	143 mJ/cm^2	143 mJ/cm^2
Laser damage threshold	200 mJ/cm^2	380 mJ/cm^2	380 mJ/cm^2

Downloaded 06 May 2002 to 132.204.56.47. Redistribution subject to AIP license or copyright, see http://ojps.aip.org/japo/japcr.jsp

IV. THEORETICAL MODELS OF AN IDEAL SPHERICAL PARTICLE ON A SMOOTH SURFACE

A. Adhesion model

The interaction forces between solids, which cause the adhesion of particles to the substrate surface, can be classified into long and short range.[9] Long-range forces, which act to bring the particle to the surface and establish the adhesive contact area, include van der Waals, capillary, electrostatic, and double-layer forces. Short-range forces, which can add to adhesion only after the establishment of an adhesive contact area, include the various types of chemical bonds: metallic, covalent, and ionic, as well as hydrogen bonds. In our previous study,[16,18] it was demonstrated that, for submicron-sized particles on hydrophilic silicon surfaces, the dominant long-range adhesion force is the van der Waals interaction, while hydrogen bonding makes the most important short-range contribution to inorganic oxide particles.

The following discussion, which assumes that particles are ideal spheres and are already in contact with a smooth substrate surface, also assumes that there is no aggregation. Van der Waals attractive forces can be calculated using a macroscopic approach,[19] in which the material properties are related to the Lifshitz–van der Waals constant. For a spherical particle and a smooth flat substrate surface, it can be expressed as[11]

$$F^v = F_0^v + F_{\mathrm{Deform}}^v = \frac{h\varpi_{132} r_p}{8\pi z_0^2} + \frac{h\varpi_{132} a^2}{8\pi z_0^3}. \tag{1}$$

The first term of Eq. (1) is the van der Waals forces between a sphere and a flat surface before deformation, and the second term is the force acting on the contact area due to elastic or plastic deformation. $h\varpi_{132}$ is the Lifshitz–van der Waals constant, r_p is the particle radius, z_0 is atomic separation distance between particle and substrate, which is not measurable but assumed to range from 0.4 to 1 nm[9] (we used $z_0 = 0.4$ nm), a is the radius of the deformation area on the particle which can be calculated for rigid particles (SiO_2 and Al_2O_3) using the JKR model.[20]

$$a^3 = \tfrac{9}{2} W \pi r_p^2 \left(\frac{1-\nu_1^2}{E_1} + \frac{1-\nu_2^2}{E_2} \right), \tag{2}$$

where W is the work of adhesion of the particle on the substrate surface whose value approaches $2(\gamma_1^s \gamma_2^s)^{1/2}$, and γ_1^s and γ_2^s are the surface free energies of particle and substrate, respectively. v and E are Poisson's ratio and Young's modulus, respectively, and their subscripts refer to particle and substrate. For PSL particles, the contact radius is not a function of the particle radius to the 2/3 power but is, rather, a function of the square root of the particle radius.[21] The PSL contact radius slowly increases with residence time;[22] we ignored these changes in our calculations because the residence time was less than three hours in our experiments, too short to cause a noticeable change.[22] During steam cleaning, particles were covered with a condensed water vapor film. The shielding effect of the liquid greatly reduces the van der Waals forces;[9] for example, the Lifshitz–van der Waals constant of Al_2O_3 particles on silicon surfaces is reduced from 5.62 to 2.23 eV.[12]

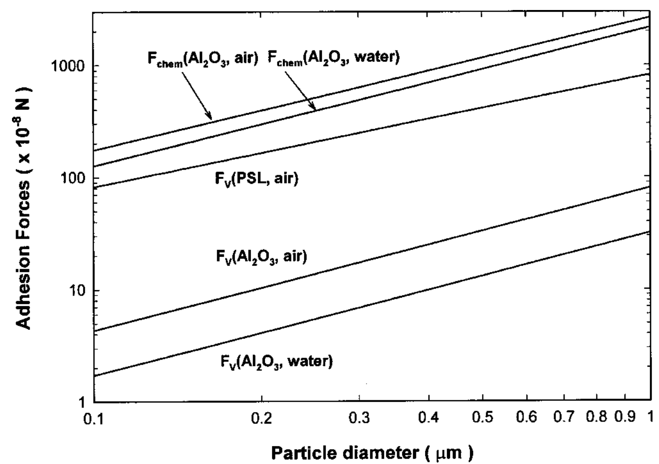

FIG. 4. Adhesion forces (van der Waals F_v and hydrogen bonding F_{chem}) of PSL and Al_2O_3 particles on a hydrophilic silicon surface during dry and steam cleaning, as a function of particle diameter.

The adhesion force due to hydrogen bonding between inorganic particles and the hydrophilic silicon surface has been discussed in our previous study.[18] It is given by

$$F_{\text{H-bond}} = DE_{\text{bond}}(\pi a^2 + 2\pi r_p \Delta z b)/d_{\text{bond}}, \tag{3}$$

where D is the OH group density on the particle surface (12.5 OH/nm^2 for Al_2O_3)[23] and E_{bond} is the hydrogen bonding interaction energy between particle and substrate. E_{bond} depends on the natures of the surfaces, particularly on their degrees of hydroxylation and on the electronic structures of the materials.[24] The average energy of the O–H- - -O hydrogen bond is about 5 kcal/mole (~0.22 eV/bond),[24] πa^2 is the deformation area of the particles, $2\pi r_p \Delta z$ is the ring area cut at a height Δz near the contact point, and b is the probability that the particle is bonded to the surface by a chain of water molecules; for Al_2O_3 on dry cleaning, $\Delta z b$ is ~0.705 nm.[18,25–27] During steam cleaning, free water molecules may break the hydrogen bond chain connecting the particle to the surface, so the probability b is reduced to, say, 50%.

d_{bond} is the hydrogen bond dissociation distance. The force constant for this bond is 0.69 N/cm.[28] Assuming this value to be constant with bond length elongation,[18] 0.1 nm is a reasonable length for the dissociation distance in our calculation, as previously noted,[18,29] and we used this value in our calculation. However, the dissociation distance can greatly affect the calculated results of the total adhesion force due to hydrogen bonds. It may, for example, be shorter than 0.1 nm; we found that a dissociation distance 30% shorter will increase the calculated adhesion force about 40%. There are other parameters that can induce calculation errors, such as the degrees of hydroxylation on particle and substrate surfaces and the presence of asperities on the surfaces. Here, we use complete hydroxylation although, in practice, it may be less. For PSL particles, there are no surface groups capable of participating in hydrogen bonding, so only van der Waals forces play a role.

Using Eqs. (1)–(3), we calculated the adhesion forces as a function of particle diameter for a typical organic particle (PSL during dry cleaning), and for a typical inorganic oxide particle (Al_2O_3 during both dry and steam cleaning), contact-

Downloaded 06 May 2002 to 132.204.56.47. Redistribution subject to AIP license or copyright, see http://ojps.aip.org/japo/japcr.jsp

ing a hydrophilic silicon surface. They are shown in Fig. 4. It appears that the adhesion forces are almost linear functions of particle diameter; they are greatly reduced during steam cleaning, and hydrogen bonding between Al_2O_3 particles and the hydrophilic silicon surface becomes much stronger than van der Waals interactions. This, and not the van der Waals force, causes the large difference in cleaning efficiencies of Al_2O_3 and PSL particles during dry laser cleaning. Indeed, the van der Waals forces acting on the Al_2O_3 particles are much less than those acting on the PSL particles, due to their smaller deformation.

B. Model for dry laser cleaning

On laser pulse irradiation during dry cleaning, both the particle and the silicon substrate absorb laser energy and are rapidly heated. The thermoelastic effect[30] causes an extremely rapid thermal expansion of the substrate and particle, which ejects the particles from the surface. In order to calculate the thermoelastic removal force, we must first know the temperature increase of both the particle and the silicon substrate due to the laser irradiation.

At the KrF excimer laser wavelength of 248 nm, the photon absorption length α^{-1} (5.5 nm)[31] and the heat diffusion length $(\kappa\tau/\rho C_p)^{1/2}$ (4.3 μm)[32,33] of silicon are much smaller than both the thickness of the wafer (0.5 mm) and the dimension of the laser beam ($0.8\,\mathrm{mm}\times 18\,\mathrm{mm}$), where α, κ, ρ, C_p, and τ are the optical absorption coefficient, the thermal conductivity, the density, the specific heat of the substrate material, and the laser pulse duration, respectively. Thus, the semi-infinite, one-dimensional heat equation is a good approximation. The temperature distribution in the substrate can then be described by[32]

$$\rho C_p(T)\frac{\partial}{\partial t}T(z,t)=\frac{\partial}{\partial z}\left[\kappa(T)\frac{\partial}{\partial z}T(z,t)\right]+(1-R)\alpha_0(t)e^{-az}, \tag{4}$$

where z is the coordinate normal to the substrate surface ($z=0$), t is the time following the laser pulse arrival, T is the temperature, R is the surface reflectivity, and $I_0(t)$ is the laser intensity. The spatial dependence of $I_0(t)$ is neglected because the particles of interest are much smaller than the laser spot. Heat conduction from the substrate surface to the ambient air is very slow, and the radiation losses are much smaller than the incident laser energy. For example, at a surface temperature of 850 K and a laser flux of 310 mJ/cm^2, the power flux into the substrate is $J_{\mathrm{in}}=-\kappa(dT/dz)=1.45\times 10^9$ W/m^2 (Ref. 34) but the power flux lost by radiation is $J_{\mathrm{rad}}=5.67\times 10^4\ T_s^4=2.32\times 10^4$ W/m^2 (Ref. 34) and by convection with the ambient air, $J_{\mathrm{conv}}=h_c(T_s-T_0)=2\times 10^4$ W/m^2,[33] where T_s and T_0 are the surface temperature and the room temperature, h_c is the unit thermal conductance (5–25 W/m^{2}K for air convection).[34] Thus, over the short time scale considered, heat losses at the substrate surface may be neglected. The boundary and initial conditions thus become

$$\left.\frac{\partial T(z,t)}{\partial z}\right|_{z=0}=0, \tag{5}$$

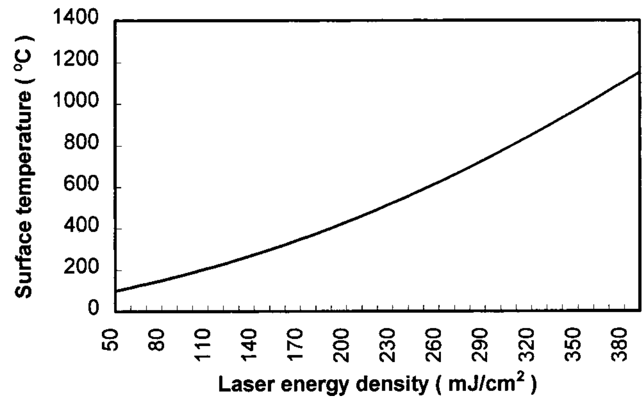

FIG. 5. Surface temperature of a silicon substrate as a function of laser energy density.

$$T(z,t)|_{z=\infty}=T(z,0)=T_0, \tag{6}$$

where T_0 is room temperature. Because the optical absorption coefficient α of crystalline silicon is very large ($1.81\times 10^6\ \mathrm{cm}^{-1}$),[31] and α and R do not change much with temperature, we employed their room temperature values in our calculation. The thermal properties of crystalline silicon strongly depend on the temperature. Using a nonlinear regression of experimentally determined[33] crystalline silicon thermal properties, $\kappa(T)$ and $C_p(T)$ can be expressed as

$$\kappa(T)=2.99\times 10^4/(T-99)\quad \mathrm{W/mK}, \tag{7}$$

$$C_p(T)=863.3+0.09923T-6369e^{-0.01216T}\quad \mathrm{J/kgK}. \tag{8}$$

The one-dimensional conductive heat transfer Eq. (4) was solved numerically by an implicit finite difference algorithm.[35] The peak surface temperature of the silicon substrate is shown in Fig. 5 as a function of laser energy density.

The calculation of the temperature distribution in particles is a very complex problem because of the nonuniform surface absorption due to small particle Mie-type scattering[36] and the difficulty of solving the three-dimensional, spherical coordinate, heat diffusion equation. Fortunately, the optical absorption lengths α^{-1} of the particles considered are $10-10^2$ μm,[37–39] much larger than the dimensions of the particles. The heat transfer from the substrate to the particles can then be ignored because of poor coupling between them so the temperature increase in the particle during laser irradiation is not significant, and we can assume that the submicron-sized particles maintain a constant temperature during laser irradiation.

The rapid temperature rise in the substrate, induced by the laser pulse, generates stresses and strains in the irradiated area. These strains cause some particle displacement. From the point of view of the particles, their resistance of these strains subjects them to ejection forces from the substrate surface equal to the stresses in the substrate.[40] If the particles are to be detached from the surface, they must experience a real displacement. Based on the relationship between stresses and strains,[30] an expression for the thermal removal force on the particles produced by substrate thermal expansion can be obtained

Downloaded 06 May 2002 to 132.204.56.47. Redistribution subject to AIP license or copyright, see http://ojps.aip.org/japo/japcr.jsp

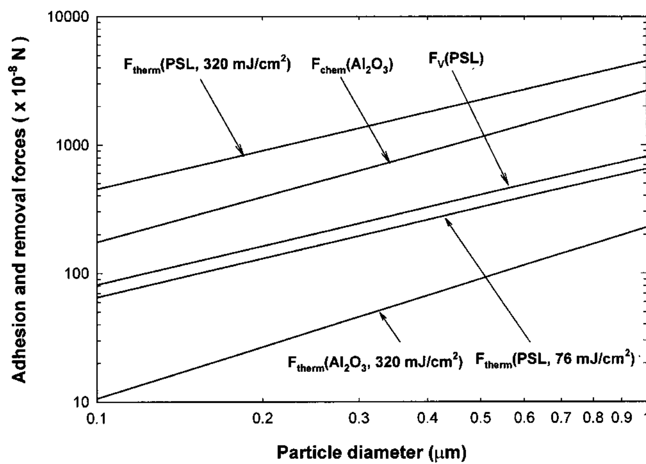

FIG. 6. Thermal removal forces F_{them} and dominant adhesion forces (van der Waals F_v and hydrogen bonding F_{chem}) as a function of particles diameter for PSL and Al_2O_3 particles during dry cleaning at laser flux of 320 and 76 mJ/cm^2 (dry cleaning threshold for PSL particles).

$$F_{\text{thermal}}=\gamma E \pi a^2 \Delta T, \tag{9}$$

where γ, E, and ΔT are the linear thermal expansion coefficient, the elastic modulus, and the temperature increase at the substrate surface, and πa^2 is the deformation area of the particle. Because the thermal removal force depends on the deformation area of the particle, soft particles such as PSL should suffer much stronger removal forces from the substrate than hard particles, such as SiO_2 and Al_2O_3. Figure 6 shows the removal forces on PSL and Al_2O_3 particles due to the thermoelastic effect under dry cleaning conditions (the incident laser energy density is about 320 mJ/cm^2) and the cleaning threshold for PSL particles (the incident laser energy density is 76 mJ/cm^2) as a function of the particle diameter. The dominant adhesion forces are also included in Fig. 6 for comparison purposes. It is apparent in that figure that the thermal removal force is large enough to overcome the adhesion forces for PSL particles under these cleaning conditions although it is much less than the hydrogen bonding forces in the case of Al_2O_3 particles. The removal force for PSL at the cleaning threshold is slightly lower than the adhesion force; only those particles, which are loosely held at the surface, can be removed. These predictions are consistent with the dry laser cleaning experiments.

The localized removal of PSL particles during dry cleaning is due to the fact that, in the irradiated area, the amplitude of the thermoelastic pulse and the coupling of stress and strain into the particles are much stronger than those of the PAW which is excited by this thermoelastic pulse. Therefore, the effective removal of PSL particles during dry cleaning is localized in the laser beam.

The absorption coefficient of PSL is $6.3\times 10^3\ \text{cm}^{-1}$.[15] Thus, during dry cleaning, the 0.1 μm PSL particles are heated predominately by energy transferred from the substrate surface, and not by the direct absorption of laser energy. The heat diffusion length $(\kappa\tau/\rho C_p)^{1/2}$ of PSL is about 0.37 μm (much larger than its diameter), where κ, ρ, and C_p are the thermal conductivity, the density and the specific heat of PSL, respectively, and τ is the duration of the substrate surface temperature over 100 °C ($\tau\sim 100$ ns, at a laser flux of 154 mJ/cm^2). PSL particle melting and ablating may then also contribute to particle removal because PSL has both a low melting point (240 °C)[41] and a low ablation threshold for the KrF laser (250 mJ/cm^2).[42]

C. Model for steam laser cleaning

In the case of steam cleaning, the water film is transparent to the excimer laser. The laser energy is absorbed only by the substrate. The rapidly heated substrate surface superheats the water layer adjacent to it, causing bubble nucleation.[43] This is followed by the creation of a dense population of bubbles which coalesce in large numbers and, in this way, an insulating vapor layer at the water/substrate interface is generated; the phenomenon is called film boiling.[43] A detailed description of the explosive evaporation of the water film is extremely difficult, due to the formation of a superheated liquid, the thermal instability of the bubbles and the development of nucleation centers.[44] The incident laser energy density (10^2 mJ/cm^2) is much larger than the heat energy density needed to heat liquid water to boiling (10^{-3} mJ/cm^2) and to vaporization (10^{-2} mJ/cm^2).[45] The vapor layer isolates the heat continuously transferring from substrate to liquid water, so that the temperature distribution in the substrate is approximately the same as that during dry cleaning.

The generation of substantial pressure due to bubble collapse, which often causes undesirable cavitation damage on propeller blades, pumps, and hydraulic machines, has been known for many years,[46] it can also be used to remove particles from solid surfaces, such as during ultrasonic and megasonic cleaning.[47] During the ablation of a liquid film by a short-pulsed laser, the pressure production is ascribed to the explosive growth of bubbles by instantaneous heating.[48,49] This bubble growth in the fluid medium generates an explosive blast wave whose shock front is perpendicular to the direction of the wave motion. The pressure jump of this shock is from atmospheric pressure P_{atm} to the shock-generated pressure P_{shock}. The pressure increment $P_{\text{shock}}-P_{\text{atm}}$ is termed the overpressure P_{over}. When a blast wave impinges perpendicularly on an unyielding surface, the movement of the shock front is terminated abruptly, normal reflection occurs and the entire front is instantly subjected to a reflected overpressure P_{reflect} which is substantially greater than the overpressure P_{over} in the immediate surrounding. The reflected overpressure is given by[50]

$$P_{\text{reflect}}=P_{\text{shock}}(8P_{\text{shock}}-P_{\text{atm}})/(P_{\text{shock}}+4P_{\text{atm}}). \tag{10}$$

During steam cleaning, the blast wave generated during the explosive growth of bubbles imposes a dynamic load on the particles in this field, which is characterized by a rapidly attained peak value, the reflected overpressure,[50] followed by a decay which accompanies the decay in the blast wave, itself.

We have made several assumptions in calculating the removal force due to bubble generation, in order to simplify the problem: (1) the shock-generated pressure is approximately equal to the vapor pressure in the vapor layer at the water/substrate interface, i.e., $P_{\text{shock}}\approx P_v(T)$; T is the tem-

Downloaded 06 May 2002 to 132.204.56.47. Redistribution subject to AIP license or copyright, see http://ojps.aip.org/japo/japcr.jsp

perature in the vapor layer, and the values of $P_v(T)$ and P_{atm} can be found in Ref. 45; (2) the temperature in the vapor layer is approximately equal to the temperature at the substrate surface; (3) the pressure inside the vapor layer is taken as the saturation vapor pressure of the superheated vapor layer due to the nonuniform temperature distribution in the liquid film;[51] and (4) the vapor layer thickness, limited by the thickness of the superheated liquid layer, may exceed the particle radius since the thermal penetration depth in water is of the order of 1 μm. The upper limit of the removal force due to bubble generation is then given by

$$F_{\mathrm{bubble}}=\pi r_p^2 P_{\mathrm{reflect}}, \tag{11}$$

where r_p is the radius of the particle.

Lu *et al.*[15] have proposed a different equation to calculate the removal force induced by bubble generation. It is based on several assumptions: (i) bubble generation is an inertia-controlled process; (ii) in the region near the liquid/substrate interface, the vapor layer created by the evaporation of the liquid acts as a plane piston, compressing the adjacent liquid and generating stress waves; (iii) the value of the volume fraction of vapor inside the superheated liquid layer is less than 1; (iv) the expansion velocity of the vapor layer is equal to the growth velocity of the bubbles; and (v) identical to (3), earlier. They deduced the pressure of the stress wave from its average energy at a unit area vapor/liquid interface, and then obtained the cleaning force induced by bubble generation

$$F_c=\{(8/3)c^2\rho f^2[P_v(T)-P_\infty]^3\}^{1/4}\pi r_p^2, \tag{12}$$

where c is the transmission speed of the stress wave, ρ is the density of the liquid, f is the volume fraction of the vapor, and P_v and P_∞ are the vapor pressure inside the bubble and the ambient liquid pressure, respectively. From this equation, they could predict the laser fluence cleaning threshold and interpret the experimental results of the removal of alumina particles from a nickel–phosphorus surface, using isopropyl alcohol.

The removal forces due to bubble generation, calculated by both models as a function of Al_2O_3 particle diameter under steam cleaning conditions (the incident laser energy density is about 150 mJ/cm^2), are given in Fig. 7. We take $f=1$ and the transmission speed of the stress wave $c=1465$ m/s, the speed of sound in water, because they are close if the stress pressure is less than 10^8 Pa.[52] Both the removal force due to the thermoplastic effect and the dominant adhesion force due to hydrogen bonding are also shown in Fig. 7.

The removal forces of the two models for 0.1 μm particles, as function of the laser energy density, are given in Fig. 8. The inflection, at a laser fluence of 180 mJ/cm^2, is due to attaining the critical temperature of water vapor and the ensuing phase transition from water vapor to an ideal gas. The figure shows that the removal force of the explosion model of Eq. (11) is about two times greater than that of Lu, *et al.* in Eq. (12), under steam laser cleaning conditions. This difference may be due to the different assumptions made in these two models: in the Lu *et al.* model, bubble generation is considered to be a reversible piston process while, in the explosion model, it is clearly irreversible. For lower vapor pressures (i.e., at lower laser flux and surface temperature), bubble generation occurs farther away from the explosive process and the values of the two models are closer. The actual bubble generation process is probably somewhere between these two models, closer to the explosion model under steam laser cleaning conditions. Unfortunately, the assumptions used in both models preclude a direct comparison with experiment. Fortunately, the resultant forces, seen in Fig. 7, are similar in magnitude.

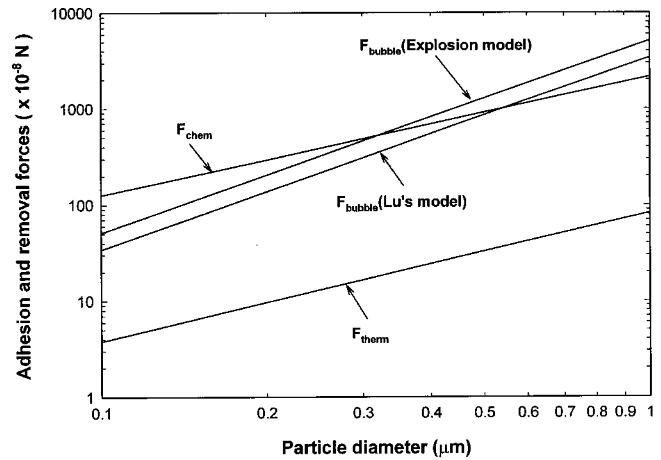

FIG. 7. Thermal removal force F_{them}, bubble removal force F_{bubble}, and dominant adhesion force F_{chem} as a function of the particle diameter, for Al_2O_3 particles during steam cleaning with a laser flux of 150 mJ/cm^2.

It is clear from Fig. 7 that the explosive evaporation of the water film generates a strong removal force, much greater than the thermal expansion force. This is so because, first, the bubble pressure has a much larger interaction area at the particle surface ($8\times10^{-3}\,\mu$m^2, as compared to $6\times10^{-5}\,\mu$m^2 for 0.1 μm Al_2O_3 particles in the purely thermoplastic regime); second, bubble generation has a much higher energy conversion efficiency (0.0015%, as compared to 0.00036% in the purely thermoelastic regime).[42] This

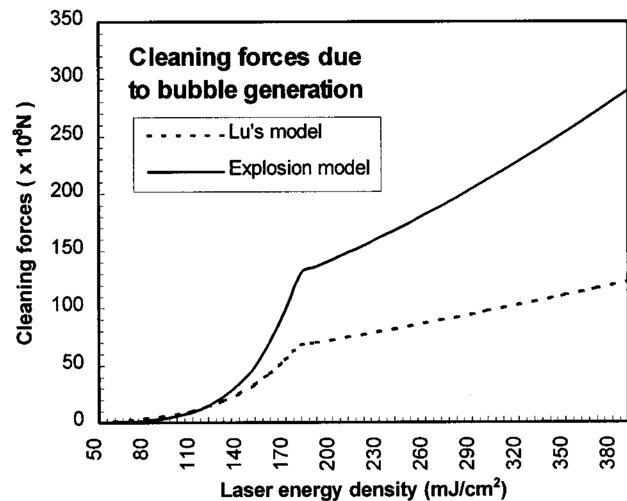

FIG. 8. The bubble generation cleaning forces of the Lu *et al.* and explosion models for 0.1 μm particles as a function of the laser energy density.

Downloaded 06 May 2002 to 132.204.56.47. Redistribution subject to AIP license or copyright, see http://ojps.aip.org/japo/japcr.jsp

analysis explains the high cleaning efficiencies of Al_2O_3 particles during steam cleaning. Because the heated area is located in the laser beam where the liquid film can explosively evaporate, only the particles in the laser beam experience the bubble pressure removal force.

A similar PAW measurement phenomenon was found for the removal of Al_2O_3 particles during steam cleaning: only the particles in the directly irradiated area were removed. As mentioned earlier, the dominant Al_2O_3 particle removal force during steam cleaning is bubble pressure. The heat diffusion length $(\kappa\tau/\rho C_p)^{1/2}$ of silicon is less than 10 μm, which can be ignored compared with the laser beam width (~1 mm). Thus, bubble generation due to superheating the water film adjacent to the substrate surface is confined to the laser beam.

In Fig. 7, we find that the removal forces due to bubble generation are still lower than the hydrogen bonding adhesion force for the particles smaller than 0.4 μm. In the next section, we will discuss the influence of surface roughness on the cleaning efficiency. The effect of surface roughness is to greatly reduce the adhesion forces.

In earlier papers,[16,17] we noted that the excimer laser energy, 5 eV, is much higher that the strength of a hydrogen bond, ~0.2 eV, and could conceivably participate in bond breaking. However, further consideration has led us to the fact that the quantized annihilation of a photon must be matched to another process (or series of processes, as in x-ray photoelectron spectroscopy) which entirely use the energy released. A review of possible processes (internal electronic transitions, ionization potentials) does not reveal a match, effectively excluding the participation of photons in hydrogen bond breaking.

V. THEORETICAL MODELS APPLIED TO REAL PARTICLES ON A REAL SILICON SURFACE

A. Surface roughness and particle aggregation

The previous particle adhesion and removal models were based on the assumption that particles are ideal spheres and that substrates have smooth, flat surfaces. However, many types of particles have irregular shapes and most substrate surfaces have a certain roughness; it has been shown that the surface roughness of a particle markedly decreases the adhesion forces.[9,53–55] We measured the surface roughness of silicon wafers by atomic force microscopy (TopoMetrix TMX 2010) and found that the average roughness was about 0.33 nm and the rms roughness was about 0.4 nm, both much smaller than the dimensions of particle asperities; thus, our substrate surface can be considered to be smooth. On the other hand, it is very difficult to measure the surface roughness of submicron-sized particles, and different particles have different surface topographies. The scanning electron microscope (SEM) and transmission electron microscope (TEM) are useful tools in determining particle surface topography. SEM photomicrographs of Al_2O_3 and SiO_2 particles are shown in Figs. 9(a) and 9(b), respectively, where we can see that the particles are elongated and rough, as well as aggregated. A similar photomicrograph of PSL particles shows them to be spherical and smooth, with no aggregation; a TEM photomicrograph of a single PSL particle is seen in Fig. 9(c). The radii of curvature of asperities r_e are much smaller than the overall radius of the particle r_p, 10% of the particle radius being a reasonable assumption for the upper limit of the asperity curvature radius; i.e., $r_e = 0.1 r_p$.

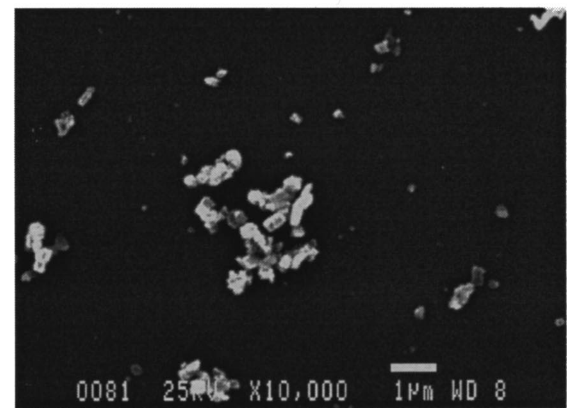

(a)

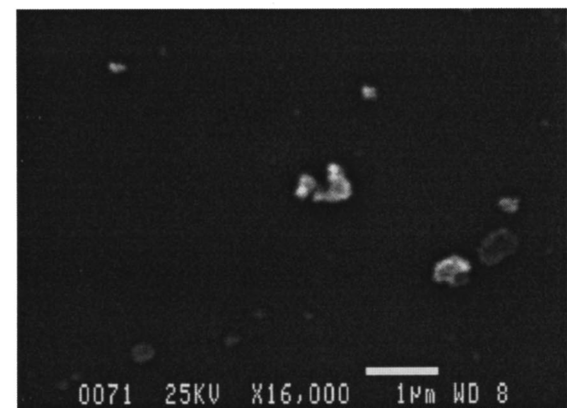

(b)

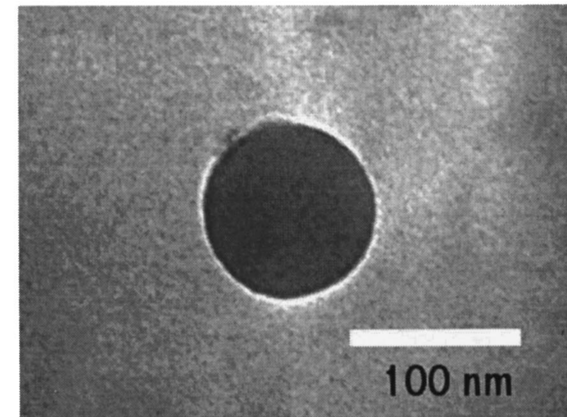

(c)

FIG. 9. Photomicrographs of 0.1 μm particles after deposition: (a) Al_2O_3 by SEM, (b) SiO_2 by SEM, and (c) PSL by TEM.

We also see that larger SiO_2 and Al_2O_3 particles are formed by the clustering of smaller ones. This aggregation appears to be the result of van der Waals attraction and hydrogen bonding, which hold particles together at the moment of contact during particle deposition.[24] The aggregation of Al_2O_3 particles is more significant than that of SiO_2 because

Downloaded 06 May 2002 to 132.204.56.47. Redistribution subject to AIP license or copyright, see http://ojps.aip.org/japo/japcr.jsp

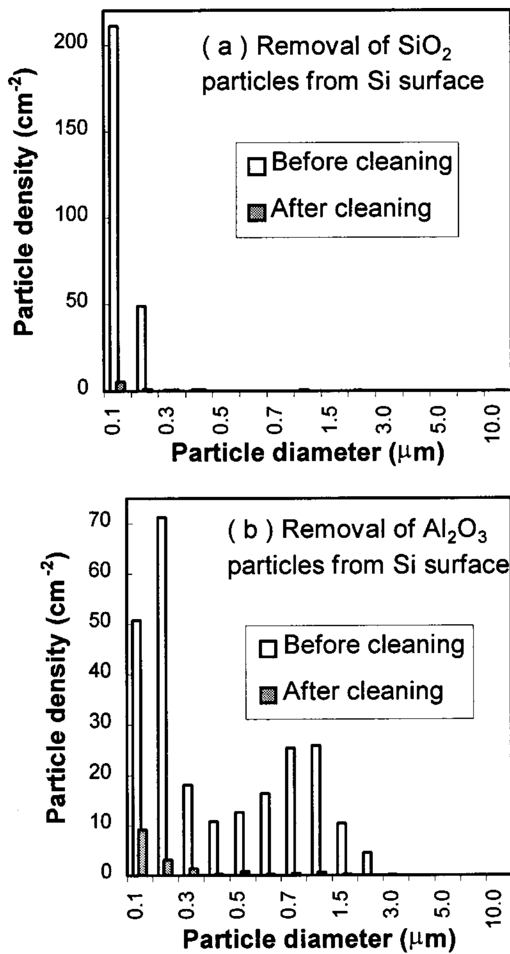

FIG. 10. Particle densities before and after steam laser cleaning; (a) SiO_2 particles, laser energy flux of 180 mJ/cm^2, 5 cleaning cycles; (b) Al_2O_3 particles, laser energy flux of 154 mJ/cm^2, 4 cleaning cycles.

Al_2O_3 has stronger hydrogen bonds (127 mdyn for 0.1 μm Al_2O_3 particles in water, 69 mdyn for 0.1 μm SiO_2 particles in water), and can form stronger and more stable links between particles. This is why the Al_2O_3 particles have a broader size distribution than SiO_2 after deposition of nominal 0.1 μm particles, as shown in Fig. 10. The peak maximum for 0.1 μm Al_2O_3 particles appears at 0.2 μm. This may be due to particle aggregation during the deposition process or to the measurement error of the laser scanning surface inspection system. The particle size distribution is optically calculated by the laser scanning surface inspection system, which is calibrated with 0.1 μm standard polystyrene latex particles;[56] substantially different optical constants for the particulate matter will lead to an erroneous size distribution.

B. Modified adhesion and laser cleaning models

It is generally recognized that surface roughness acts to reduce the adhesion between two solids. When the radii of the asperities at the particle surface are much greater than the particle-substrate separation, the effective particle radius and contact area that appear in Eqs. (1)–(3) and (9) must be decreased. This is because the dominant component of the force between particle and substrate surface acts only at the contact points and the surrounding areas. In general, there is no predictable relationship between the geometry of the surface asperities and the overall particle radius. To simplifying the problem, the rough particle is modeled by a spherical solid core having uniformly distributed spherical asperities on the surface, all with the same radius of curvature r_e and height. In the stable state of a single particle contacting the substrate, there are either three or four asperities in contact with the substrate surface. We selected average 3.5 contact points.

TABLE II. Adhesion and removal forces for inorganic oxides with and without asperities.

Forces	Particles			
	SiO_2		Al_2O_3	
	With asperities (mdyn)	Ideal sphere (mdyn)	With asperities (mdyn)	Ideal sphere (mydn)
F^V	0.87	1.5	0.4	1.7
$F_{\text{H-bond}}$	14.7	69.6	29.8	126
F_{thermal}	1	6.7	0.7	3.8
F_{bubble}	51.4	51.4	51.4	51.4

In the case of 0.1 μm Al_2O_3 particles, the larger particle sizes are assumed to be aggregates of 0.1 μm particles. The total number of asperities contacting the substrate surface depends on the number of components and the structure of the cluster. We cannot calculate the total number of contact points because the aggregation of small particles depends on random contact processes and the possibility of forming clusters of all shapes, varying with cluster growth in a way too complex to simulate. The determination of the actual dimensions of the clusters is another problem,[56] the laser scanning surface inspection system only giving the equivalent spherical diameter of a PSL particle. The contact area between cluster and substrate surface is determined directly by the dimensions and shapes of the clusters.

The simplest calculable case is for a single 0.1 μm particle with asperities on the substrate surface. The equations to calculate the adhesion and the thermoelastic removal forces are the same as before except that, in Eqs. (1)–(3) and (9), the particle radius r_p must be replaced by the effective radius of the particles (asperity radius) r_e; this value is taken as 0.005 μm in the present case, as indicated earlier. The bubble removal force would not be affected by asperities or by aggregation because it acts over the entire bottom half of the particle; this means that Eq. (10) does not change. Using these equations, we recalculated the adhesion and removal forces for 0.1 μm irregular Al_2O_3 and SiO_2 particles on a silicon surface, during steam cleaning with a laser flux of 150 mJ/cm^2, and the results are shown in Table II; they are in agreement with experiment.

One can easily see from the table that, when asperities and aggregation are considered, the adhesion and thermoelastic removal forces are significantly decreased. The dominant adhesion force is still hydrogen bonding, and the thermoelastic removal force is larger than the van der Waals force but much smaller than the hydrogen bonding force. During steam cleaning, the removal force induced by bubble

Downloaded 06 May 2002 to 132.204.56.47. Redistribution subject to AIP license or copyright, see http://ojps.aip.org/japo/japcr.jsp

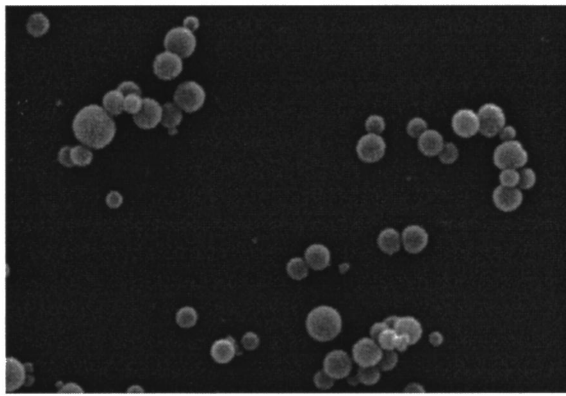

FIG. 11. SEM photomicrograph of 0.1 μm colloidal SiO_2 particles.

generation is great enough to overcome the adhesion forces and eject particles from the substrate surface. The difference in magnitude between the bubble pressure removal force and the adhesion force increases with particle diameter, and may explain why larger particles are much easier to remove from the substrate surface when asperities and aggregation are present.

Colloidal SiO_2 particles were employed in the steam cleaning experiments to confirm the influences of asperities on the cleaning efficiency. They have smooth surfaces and a more spherical shape than powdered SiO_2 particles, as seen in Fig. 11. Colloidal SiO_2 particle densities before and after steam cleaning are seen in Fig. 12. It was found that the steam cleaning efficiency of colloidal SiO_2 particles was much lower than that of powdered SiO_2, as seen in Fig. 10(a). The dominant size of both colloidal and powdered SiO_2 particles is 0.1 μm. Roughly 64% of colloidal SiO_2 particles were removed, compared to 97% of the powdered SiO_2 particles (with asperities), under similar conditions [see Fig. 10(a)]. The theoretical predictions given earlier are in good agreement with these experimental results.

The contact area of a cluster with a surface involves only some of the component particles and there are an average 3.5 asperities for each contacting component. Thus, the adhesion forces of clusters are also greatly reduced but, since the bubble removal force will not be affected, the cleaning efficiency for clusters will also be greatly improved.

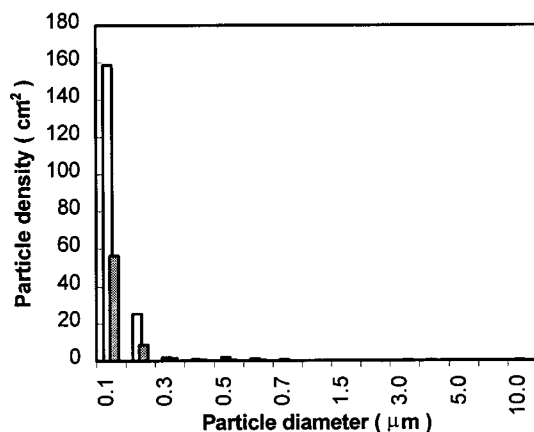

FIG. 12. Colloidal SiO_2 particle densities before and after steam laser cleaning with a laser energy flux 215 mJ/cm^2, 6 cleaning cycles.

VI. CONCLUSIONS

We offer theoretical models to explain our excimer laser cleaning results on both organic latex and inorganic oxide particles from hydrophilic silicon surfaces. Hydrogen bonding was found to be the dominant contribution to the oxide particles over the organic particles. The greated efficiency of steam cleaning, in the case of oxide particles, is shown to be due to bubble pressure. Our bubble pressure model is compared to one found in the literature; although the approximations used in their derivations preclude a direct comparison with experimental values, the forces generated by each model are almost equal in magnitude.

The effect of asperities has been considered in our models, by the replacement of the spherical particle radius with the asperity radius. The reduction in the magnitudes of the various forces explain the substantial reduction in the experimental adhesion on roughening a particle surface.

ACKNOWLEDGMENTS

The authors thank J. P. Lévesque for his technical assistance. This work was supported by the Natural Sciences and Engineering Research Council of Canada.

[1] W. Zapka, W. Ziemlich, and A. C. Tam, Appl. Phys. Lett. **58**, 2217 (1991).
[2] K. Imen, S. J. Lee, and S. D. Allen, Appl. Phys. Lett. **58**, 203 (1991).
[3] A. C. Tam, W. P. Leung, W. Zapka, and W. Ziemlich, J. Appl. Phys. **71**, 3515 (1992).
[4] J. D. Kelley, M. I. Stuff, F. E. Hovis, and G. J. Linford, Proc. SPIE **1415**, 211 (1991).
[5] H. K. Park, C. P. Grigoropoulos, W. P. Leung, and A. C. Tam, IEEE Trans. Compon. Packag. Manuf. Technol., Part A **17**, 631 (1994).
[6] F. Beaudoin, M. Meunier, M. Simard-Normandin, and D. Landheer, J. Vac. Sci. Technol. A **16**, 1976 (1998).
[7] J. B. Héroux, S. Boughaba, I. Ressejac, E. Sacher, and M. Meunier, J. Appl. Phys. **79**, 2857 (1996).
[8] S. Boughaba, X. Wu, E. Sacher, and M. Meunier, J. Adhes. **61**, 293 (1997).
[9] H. Krupp, Adv. Colloid Interface Sci. **1**, 111 (1967).
[10] J. A. Kitchener, J. Soc. Cosmet. Chem. **24**, 709 (1973).
[11] R. A. Bowling, J. Electrochem. Soc. **132**, 2209 (1985).
[12] M. B. Ranade, Aerosol Sci. Technol. **7**, 161 (1987).
[13] J. D. Kelley and F. E. Hovis, Microelectron. Eng. **20**, 159 (1993).
[14] Y. F. Lu, W. D. Song, B. W. Ang, M. H. Hong, D. S. H. Chan, and T. S. Low, Appl. Phys. A: Mater. Sci. Process. **65**, 9 (1997).
[15] Y. F. Lu, Y. Zhang, W. D. Song, and D. S. H. Chan, Jpn. J. Appl. Phys., Part 2 **37**, L1330 (1998).
[16] X. Wu, E. Sacher, and M. Meunier, J. Adhes. **70**, 167 (1999).
[17] X. Wu, E. Sacher, and M. Meunier, *Proc. 22nd Annu. Mtg. Adhesion Soc.* (Adhesion Society, Blacksburg, VA, 1999), p. 277.
[18] X. Wu, E. Sacher, and M. Meunier, J. Appl. Phys. **86**, 1744 (1999).
[19] E. M. Lifshitz, Sov. Phys. JETP **2**, 73 (1956).
[20] K. L. Johnson, K. Kendall, and A. D. Roberts, Proc. R. Soc. London, Ser. A **324**, 301 (1971).
[21] D. S. Rimai and L. P. Demejo, Annu. Rev. Mater. Sci. **26**, 21 (1996).
[22] S. Krishnan, A. A. Busnaina, D. S. Rimai, and L. P. Demejo, J. Adhes. Sci. Technol. **8**, 1357 (1994).
[23] J. J. Kipling and D. B. Peacall, J. Chem. Soc. **182**, 834 (1957).
[24] P. K. Iler, *The Chemistry of Silica* (Wiley-Interscience, New York, 1970), pp. 373 and 387.
[25] *CRC Handbook of Chemistry and Physics* edited by D. R. Lide and H. P. R. Frederikse (CRC Press, New York, 1996), pp. 9–22.

Downloaded 06 May 2002 to 132.204.56.47. Redistribution subject to AIP license or copyright, see http://ojps.aip.org/japo/japcr.jsp

[26] M. D. Joesten and L. J. Schaad, *Hydrogen Bonding* (Marcel Dekker, New York, 1974), pp. 36 and 38.
[27] I. Olovsson and P. Jonsson, in *The Hydrogen Bond*, edited by P. Schuster, G. Zandel, and C. Sandorfy (North-Holland, New York, 1976), Chap. 8.
[28] P. Schuster, in *The Hydrogen Bond*, edited by P. Schuster, G. Zandel, and C. Sandorfy (North-Holland, New York, 1976), p. 40.
[29] J. Israelachvili, *Intermolecular and Surface Forces* (Academic, New York, 1991), Chap. 8.
[30] D. Burgreen, *Elements of Thermal Stress Analysis* (C. P. Press, Jamaica, NY, 1971), pp. 77, 129, and 179.
[31] D. E. Aspnes and A. A. Studna, Phys. Rev. B **27**, 985 (1983).
[32] P. Baeri and S. U. Campisano, in *Laser Annealing of Semiconductors*, edited by J. M. Poate and J. W. Mayer (Academic, New York, 1982), Chap. 4.
[33] *Thermophysical Properties of Matter* edited by Y. S. Touloukian (IFI/Plenum, New York 1970, 1973, 1977), Vols. 4, 5, and 13.
[34] J. P. Holman *Heat Transfer* (McGraw-Hill, New York, 1997), pp. 2, 12, 13.
[35] M. N. Ozisik *Boundary Value Problem of Heat Conduction* (International Textbook, Scranton, PA, 1968), pp. 402–405.
[36] H. Hulst, *Light Scattering by Small Particles* (Wiley, New York, 1957).
[37] S. Lazare and V. Gramier, Laser Chem. **10**, 25 (1989).
[38] K. Awazu, H. Kawazve, and K. Muta, J. Appl. Phys. **68**, 4183 (1991).
[39] B. D. Evans, J. Appl. Phys. **70**, 3995 (1991).
[40] Y. F. Lu, W. D. Song, K. D. Ye, Y. P. Lee, D. S. H. Chan, and T. S. Low, Jpn. J. Appl. Phys., Part 2 **36**, L1304 (1997).
[41] *Polymer Handbook*, edited by J. Brandrup and E. H. Immergut (Wiley-Interscience, New York, 1989), p. 82.
[42] G. Paraskevopoulos, D. L. Singleton, R. S. Irwin, and R. S. Taylor, J. Appl. Phys. **70**, 1938 (1991).
[43] S. V. Stralen and R. Cole, *Boiling Phenomena* (Hemisphere, Washington, 1979), Vol. 1.
[44] L. M. Lyamshev and K. A. Naugol'nykh, Sov. Phys. Acoust. **27**, 357 (1982).
[45] *CRC Handbook of Chemistry and Physics* edited by D. R. Lide and H. P. R. Frederikse (CRC Press, New York, 1996), pp. 6–10 and 6–16.
[46] D. H. Trevena *Cavitation and Tension in Liquids* (Adam Hilger, Bristol, 1987).
[47] J. Bardina in *Particles on Surface 1: Detection, Adhesion, and Removal*, edited by Mittal K. L. (Plenum, New York, 1988), p. 329.
[48] H. K. Park, D. Kim, C. P. Grigoropoulos, and A. C. Tam, J. Appl. Phys. **80**, 4072 (1996).
[49] O. Yavas, A. Schilling, J. Bischof, J. Boneberg, and P. Leiderer, Appl. Phys. A: Mater. Sci. Process. **64**, 331 (1997).
[50] G. F. Kinney, *Explosive Shocks in Air* (Macmillan, New York, 1962).
[51] V. P. Carey *Liquid-Vapor Phase-Change Phenomena* (Hemisphere, Washington, 1992), p. 193.
[52] G. P. Davidson and D. C. Emmony, J. Phys. E **13**, 92 (1980).
[53] D. M. Schaefer, M. Carpenter, B. Gady, R. Reifenberger, L. P. Demejo, and D. S. Rimai, J. Adhes. Sci. Technol. **9**, 1049 (1995).
[54] K. N. G. Fuller and D. Tabor, Proc. R. Soc. London, Ser. A **345**, 327 (1975).
[55] J. Czarnecki and T. Dabros, J. Colloid Interface Sci. **78**, 25 (1980).
[56] M. Ohomori, M. Yasutake, and S. Wakiyama, J. Electrochem. Soc. **143**, 4125 (1996).

Downloaded 06 May 2002 to 132.204.56.47. Redistribution subject to AIP license or copyright, see http://ojps.aip.org/japo/japcr.jsp